Nanotechnology **22** (2011) 235303 (5pp) doi:10.1088/0957-4484/22/23/235303

Multi-layer nanogap array for high-performance SERS substrate

Myeong-Lok Seol[1], Ju-Hyun Kim[1], Taejoon Kang[2], Hwon Im[1], Sungho Kim[1], Bongsoo Kim[2] and Yang-Kyu Choi[1]

[1] Department of Electrical Engineering, KAIST, Daejeon 305-701, Republic of Korea
[2] Department of Chemistry, KAIST, Daejeon 305-701, Republic of Korea

E-mail: ykchoi@ee.kaist.ac.kr

Received 16 January 2011, in final form 8 March 2011
Published 11 April 2011
Online at stacks.iop.org/Nano/22/235303

Abstract
A multi-layer nanogap array composed of three linearly aligned gold nanogaps is fabricated for a surface-enhanced Raman spectroscopy (SERS) substrate. The overall process for the proposed structure is simple and reliable with the use of a photolithography-free fabrication process, which includes only deposition and etching. Chemical vapor deposition (CVD) is employed to form a uniform and highly controllable nanogap array. The nanogap width, a crucial parameter in SERS, is determined by the sacrificial film thickness of CVD. Experiments on nanogap width and polarization angle dependence are carried out to characterize the fabricated multi-layer nanogap array as an SERS substrate.

(Some figures in this article are in colour only in the electronic version)

1. Introduction

Various metal nanostructures have been studied due to their specific electrical and optical characteristics [1–4]. Surface-enhanced Raman spectroscopy (SERS) is a powerful technique that utilizes the metal nanostructure for the purpose of chemical analysis [5–12]. High signal enhancement of SERS is caused by the localized surface plasmon resonance (LSPR) phenomenon, which occurs as light is incident on the metal surface. LSPR causes local electric field enhancement which in turn reinforces the Raman scattering intensity. Through this reinforced Raman scattering, the molecules adsorbed on the surface are able to be precisely detected and analyzed. The high sensitivity of SERS enables single-molecule detection as well [6].

For the stronger field enhancement of LSPR, a roughened metal surface is needed. Within the roughened surface, there are sites known as the 'hot spot' which is usually formed by a narrow metal nanogap. Although a flat metal surface can also generate electric field enhancement, most enhancements occur on these hot spots. Hence, it is important to develop a technique that can precisely control the geometry of the nanostructure to form hot spots with high quality. Various methods to fabricate densely filled hot spots have been developed such as the top-down lithographic patterning and the bottom-up nanoparticle aggregation [7–12].

Electron beam lithography (EBL) is the most widely used technique among the top-down fabrication methods for SERS substrates [7–10]. High resolution of EBL allows precise control of the well-ordered nanogap in the sub-100 nm scale with high uniformity. However, the major drawback of this technique is its low throughput and high fabrication cost. Each nanostructure has to be patterned one by one to make a nanogap. On the other hand, bottom-up nanoparticle aggregation can easily make an SERS substrate with densely filled hot spots [11, 12]. This technique is advantageous in that it has high throughput, but the controllability and uniformity of the structure are relatively poor. To overcome the aforementioned problems, a technique that combines the strengths of both top-down and bottom-up methods is called for.

The dielectric deposition using chemical vapor deposition (CVD) is one of the key technologies in modern nanofabrication. CVD can accurately control the thickness in the sub-10 nm dimension with ease. In this work, by using accurate controllability and uniformity of the CVD technique, a multi-layer nanogap array for an SERS substrate is fabricated. The geometry of the nanogap can be easily controlled with simple modifications in the fabrication process.

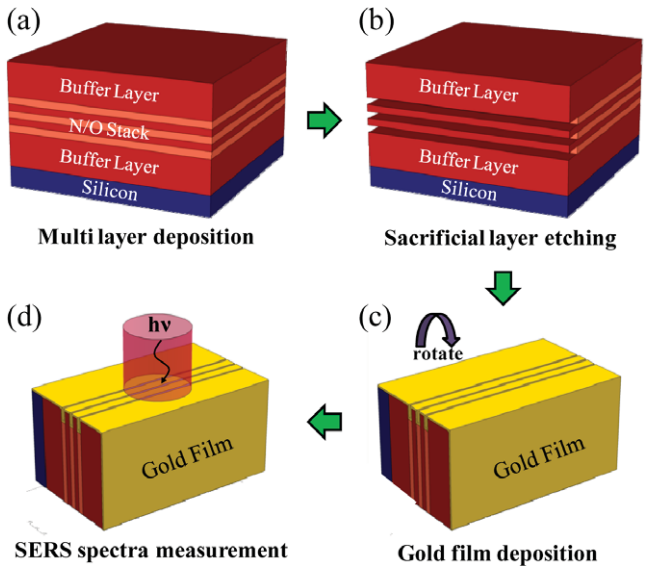

Figure 1. Schematics describing the fabrication process of the multi-layer nanogap array. (a) Deposition of the multi-dielectric layer consisting of the bottom and top buffer layers (2 μm SiO_2), supporting layers (each 100 nm SiO_2) and sacrificial layers (each 100 nm Si_3N_4). (b) Formation of the dielectric nanogap as the sacrificial layer is selectively etched. (c) Gold film deposition to form SERS active hot spot. (d) Raman spectrum measurement using the multi-layer nanogap array as SERS substrate. Red cylinder describes focusing light of 633 nm He–Ne laser. 10 μl of 10^{-6} M ethanolic solution of brilliant cresyl blue (BCB, Sigma-Aldrich) was used for drop evaporation which is used for attaching the molecules.

As this photolithography-free process only uses deposition and etching, it can be simply fabricated while maintaining high uniformity. Moreover, as deposition and etching are applied to the whole wafer, the process allows low cost and high throughput.

2. Experimental details

2.1. Fabrication of multi-layer nanogap array

Figure 1 is a schematic of the fabrication process. The fabrication begins on a 4 inch (100) silicon wafer (thickness ~525 μm). First of all, 2 μm of an SiO_2 bottom buffer layer was deposited on the wafer. This bottom buffer layer relieves the stress that occurs on the Si_3N_4 layer and allows easier laser focusing when an optical microscope is used for SERS measurement. After the bottom buffer layer was deposited, layers of Si_3N_4 and SiO_2 were deposited on top of each other five times alternately. In this step, the Si_3N_4 and SiO_2 were each sacrificial and supporting layers, respectively. Finally, a 2 μm buffer layer (SiO_2) was deposited on the top. The top buffer layer also allows easier laser focusing and serves as a passivation layer for protecting the hot spot region (figure 1(a)). All dielectric layers throughout the experiment were deposited with low-stress plasma-enhanced chemical vapor deposition (PE-CVD, UNAXIS, equipment code: NPE10) under a temperature of 350 °C.

After deposition, rectangles with dimensions of 10 mm × 7.5 mm were cleaved along the (110) face of the wafer. In this step, manual cleaving was used to form a uniform cross-sectional face. As the manual cleaving allows the wafer to be cut along the silicon crystal orientation, the exposed facet was almost perfectly flat, like a nanoscale mirror [13, 14]. Although the thick silicon layer beneath the dielectric stack does not contain any hot spot region, this layer is essential as it helps the dielectric stack to maintain a clean facet.

After cleaving, the sacrificial layer (Si_3N_4) was etched to create a nanogap. Phosphoric acid was used as the wet etchant and the etching time was 40 s. A temperature of 150 °C was maintained during etching. Estimated selectivity of nitride versus oxide is 6:1 in this experiment. According to the etching time, the depth of the nanogap can be controlled. As the thickness of the sacrificial layer is 100 nm, the initial thickness of the nanogap is 100 nm. The distance between the nanogaps is also 100 nm because the thickness of the SiO_2 layer is 100 nm. As a result, three 100 nm nanogaps that are 100 nm away from one another can be created in the form of a multi-layer nanogap array (figure 1(b)). According to the deposition thickness of the SiO_2 and Si_3N_4, one can easily control the geometric parameters of the nanogap array.

Once etching had been completed, a gold film was deposited by sputtering in order to use the above structure as an SERS-active substrate. No additional adhesion layer is used before the gold layer deposition. Although silver is preferable to gold in terms of Raman enhancement, gold is chosen due to its chemical stability and biocompatibility. The initial nanogap width, which is a crucial factor in governing the sensitivity, decreases as the gold film is deposited. Hence, by controlling the deposition time, the width of the nanogap can be adjusted. As field enhancement is sensitive to the change in the nanogap width, precise control of the deposition time is important. The final structure of a proposed multi-layer nanogap array consisting of three gold nanogaps is shown in figure 1(c).

Figures 2(a) and (b) are the schematics describing the effect of gold deposition angle. As the etching process did not show perfect selectivity, the nanogap after sacrificial layer etching has a trapezoidal shape. For this structure, the angle of gold deposition determines the resulting shape of the gold nanogap. When the deposition angle is directly perpendicular to the surface, as it is in the usual case, the side walls of the nanogap will be filled and the resulting gold nanogap will have a triangular shape (figure 2(a)). In this case, it is hard to implement a small nanogap width with a reasonable nanogap depth. On the other hand, when tilted gold deposition is used, gold film is deposited at a slower pace in the deep region of the nanogap as the adjacent supporting layer prevents the deposition of the sputtered gold atoms. Due to this shadowing effect, the depth of the nanogap can be maintained for a long deposition time (figure 2(b)). For this advantage, a tilted gold deposition method is used throughout this research. A similar approach to preserve the nanogap from metal atoms was also demonstrated in previous research [15].

2.2. SERS spectra measurement

10 μl of 10^{-6} M ethanolic solution of brilliant cresyl blue (BCB, Sigma-Aldrich) was drop-evaporated on the

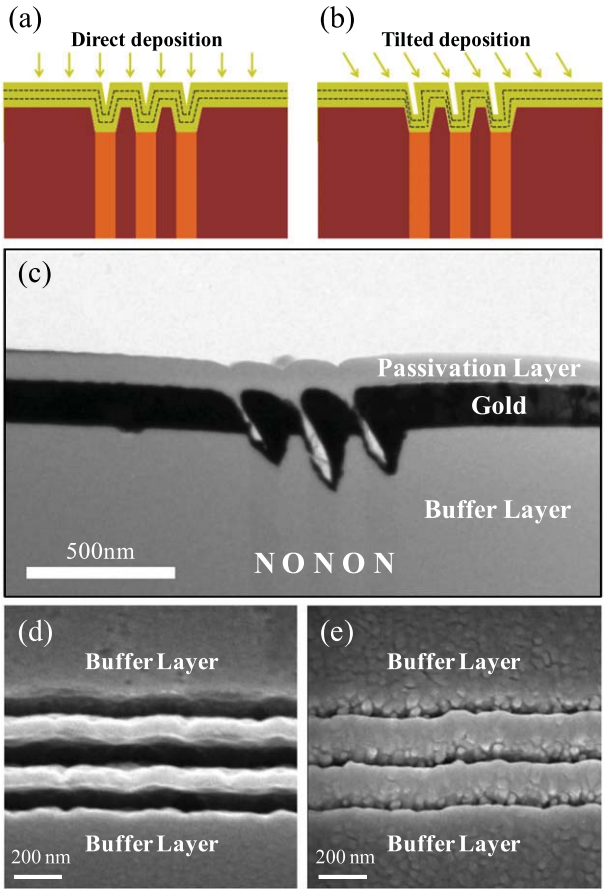

Figure 2. ((a), (b)) Schematics describing the finalized nanogap structure when (a) direct gold deposition and (b) tilted gold deposition is used. Dashed lines describe the gold film boundary when a different gold deposition time is used. (c) Transmission electron microscopy (TEM) image of multi-layer nanogap array. Tilted gold deposition is used for this structure. Top gray layer is 100 nm of silicon nitride serving as the passivation layer for focused ion beam (FIB) which is typically used for making the TEM specimen. This layer is present only in a sample for TEM analysis. ((d), (e)) Scanning electron microscopy (SEM) images of the multi-layer nanogap arrays. The average width and the mean deviation of each nanogap is (d) 85.3 ± 6. 5 nm and (e) 14.9 ± 2.1 nm, respectively. The width of the nanogap is measured at 27 random points using the SEM ruler tool.

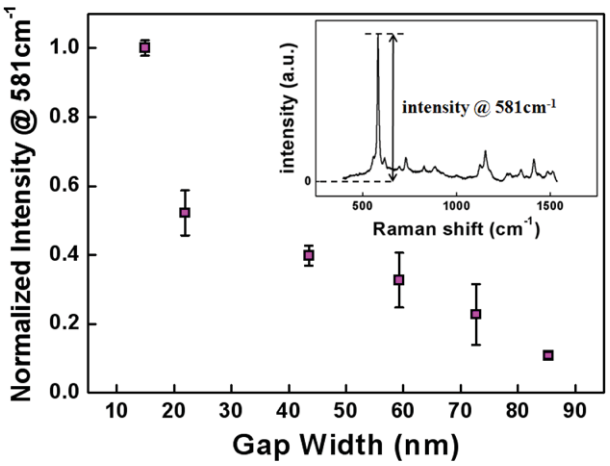

Figure 3. Comparison of the Raman enhancement according to the width of the multi-layer nanogap array. BCB molecule of 10^{-6} M was used as the target molecule. Raman intensity at 581 cm^{-1} with the maximum peak was compared. The average and standard deviation values calculated from five points for each sample are plotted. Mean deviations of the nanogap width range from a minimum value of 7% to a maximum value of 19%. Inset is the typical Raman spectrum of the BCB molecule.

multi-layer nanogap array. The SERS spectra were measured by a home-made micro-Raman system based on an Olympus BX41 microscope. A 633 nm He–Ne laser (Melles Griot) was used as an excitation source. The laser beam was focused on the sample through a 100× objective (NA = 0.7, Mitutoyo). The diameter of the laser spot is about 500 nm, which is close to the width of the multi-layer nanogap region (figure 1(d)). The light scattered from the sample was detected through a thermoelectrically cooled electron multiplying charge-coupled device (EMCCD, Andor). In this procedure, a holographic notch filter was used for laser light filtering.

3. Results and discussion

Figure 2(c) is a transmission electron microscopy (TEM) image of the fabricated multi-layer nanogap array. The effect of tilted gold deposition is shown in this image. Due to the shadowing effect, the side wall is only partially filled by gold and therefore the nanogap depth is maintained. For this structure, an average nanogap width of 14.9 nm is successfully implemented with a depth of more than 200 nm. Figures 2(d) and (e) are the scanning electron microscopy (SEM) images with different nanogap widths. The nanogap width turned out to be 85.3 ± 6.5 nm and 14.9 ± 2.1 nm, respectively. 7–19% of local variations in the nanogap width are found which are mainly caused by the roughness of the sputtered gold layer. The nanogap width is tuned by the gold deposition time. During the gold deposition process, a delicate optimization is needed for the deposition time. If the deposition time is too short, a strong hot spot cannot take place as the width cannot be small enough. On the other hand, if the deposition time is too long, the gold film covers the gap and leads to a rapid decrease in the hot spot density. It is important to find the optimum sputtering condition where we have the least width without removing the gap.

Figure 3 shows the plot of SERS intensity of the 581 cm^{-1} band according to the nanogap width. The width of the nanogap was determined by averaging 27 randomly selected points. The inset in figure 3 is the typical SERS spectrum of the BCB molecule. A major peak of the spectrum is observed at a Raman shift of 581 cm^{-1}. The major peak intensity's dependence on the nanogap width is plotted in figure 3. The SERS intensity is observed to be larger for narrower nanogap width, and maximizes at a gap of 14.9 nm. This is due to the stronger interaction induced by the LSPR in the nanogap region when the distance between the two metal films decreases. This tendency is consistent with the results from previous reports and simulations [16, 17].

The polarization dependence of the multi-layer nanogap array is plotted in figures 4(a) and (b). As the fabricated

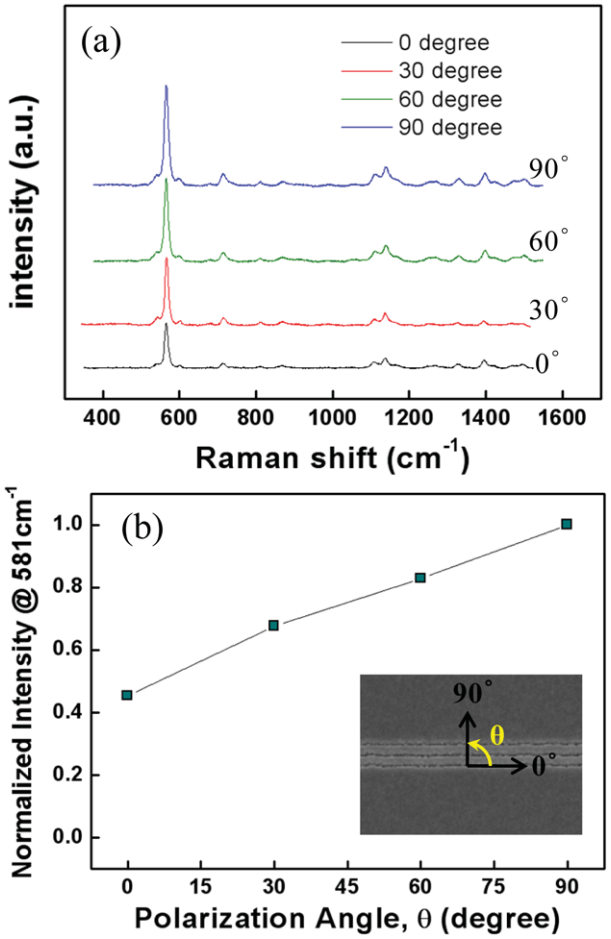

Figure 4. (a) SERS spectrum according to the polarization angle. BCB molecule of 10^{-6} M is used as the target molecule. The sample with nanogap width of 14.9 nm is used for this experiment. Each curve is vertically shifted in the y direction for easier comparison. From the bottom to top curves, the illumination was done at polarization angles of 0°, 30°, 60° and 90° when the gap direction is considered as 0°. (b) Comparison of the normalized Raman intensity at 581 cm^{-1} where each curve shows maximum peak. Inset is the SEM image for describing the polarization angle (θ).

multi-layer nanogaps are aligned linearly in one direction, it can be sensitive to the polarization direction of incident light. Figure 4(a) shows the SERS spectra of the BCB in relation to the polarization angle (θ). The SERS intensity of 581 cm^{-1} versus polarization angle (θ) is plotted in figure 4(b). The SERS intensity is largest when the polarization direction was perpendicular to the aligned direction of the nanogap and smallest when parallel. This is because the main direction of the local electric field is perpendicular to the aligned direction of the nanogap. This result is consistent with the previous reports from other laboratories as well [18–20].

The reason why the signal does not completely vanish when the polarization angle is parallel to the nanogap direction is possibly due to the partial uneven roughness of the nanogap structure. The localized electric field can be produced from many different angles according to the gold's grain size during sputtering. When a stronger dependence on polarization is needed for a particular application, uniform metal deposition techniques such as metal atomic layer deposition (ALD) can be used [21–23]. In this case, a more obvious polarization angle dependence can be obtained because the gold grain size is much smaller than for sputtering.

4. Conclusions

In summary, the multi-layer nanogap array for an SERS substrate was developed through a simple and reliable photolithography-free process. The nanogap fabrication was based on CVD technology used for nanoscale dielectric deposition. The deposited layers through CVD showed excellent thickness uniformity and controllability in wafer scale, and allowed the structure to be reproducible and to have high throughput. Moreover, with simple modifications of the fabrication process, parameters such as the number of nanogaps, the distance between nanogaps, depth of the nanogap and the nanogap width could be adjusted to meet the user's demands. From the experimental result of the nanogap width dependence, stronger signal enhancement was observed at smaller nanogap width. Also, our hypothesis that the enhancement would be strongest when the polarization angle is perpendicular to the nanogap was confirmed. We believe that the proposed multi-layer nanogap array can be utilized for the purpose of a small-sized electrochemical sensing system, and also these results will be helpful for further studies on nanogap-array-based single-molecule detection systems.

Acknowledgments

This work was supported by the National Research Foundation of Korea (NRF, 2010-0018931) and the National Research and Development Program (NRDP, 2010-0002108) for the development of biomedical function monitoring biosensors, sponsored by the Korea Ministry of Education, Science and Technology (MEST).

References

[1] Miyazaki H T and Kurokawa Y 2006 *Phys. Rev. Lett.* **96** 097401
[2] Kim J-H, Kang T, Yoo S M, Lee S Y, Kim B and Choi Y-K 2009 *Nanotechnology* **20** 235302
[3] Hou Y, Xu J, Wang P and Yu D 2010 *Appl. Phys. Lett.* **96** 203107
[4] Im H, Bantz K C, Lindquist N C, Haynes C L and Oh S-H 2010 *Nano Lett.* **10** 2231
[5] Jeanmaire D L and Van Duyne R P 1977 *J. Electroanal. Chem.* **84** 1
[6] Nie S and Emory S R 1997 *Science* **275** 1102
[7] Gunnarsson L, Bjerneld E J, Xu H, Petronis S, Kasemo B and Kall M 2001 *Appl. Phys. Lett.* **78** 802
[8] Sackmann M, Born S, Balster T and Materny A 2007 *J. Raman Spectrosc.* **38** 277
[9] Yu Q, Guan P, Qin D, Golden G and Wallace P M 2008 *Nano Lett.* **8** 1923
[10] Guillot N, Shen H, Fremaux B, Peron O, Rinnert E, Toury T and Chapelle M L 2010 *Appl. Phys. Lett.* **97** 023113
[11] Jana N R and Pal T 2007 *Adv. Mater.* **19** 1761

[12] Fang P-P, Li J-F, Yang Z-L, Li L-M, Ren B and Tian Z-Q 2008 *J. Raman Spectrosc.* **39** 1679
[13] Natelson D, Willett R L, West K W and Pfeiffer L N 2000 *Appl. Phys. Lett.* **77** 1991
[14] Luber S M, Strobel S, Tranitz H-P, Wegscheider W, Schuh D and Tornow M 2005 *Nanotechnology* **16** 1182
[15] Melosh N A, Boukai A, Diana F, Gerardot B, Badolato A, Petroff P M and Heath J R 2003 *Science* **300** 112
[16] Hao E and Schatz G C 2004 *J. Chem. Phys.* **120** 357
[17] Mu C, Zhang J-P and Xu D 2010 *Nanotechnology* **21** 015604
[18] Jeong D H, Zhang Y X and Moskovits M 2004 *J. Phys. Chem.* B **108** 12724
[19] Wei H, Hao F, Huang Y, Wang W, Nordlander P and Xu H 2008 *Nano Lett.* **8** 2497
[20] Kang T *et al* 2009 *J. Phys. Chem.* C **113** 7492
[21] Utke I, Hoffmann P, Dwir B, Leifer K, Kapon E and Doppelt P 2000 *J. Vac. Sci. Technol.* B **18** 3168
[22] Lim B S, Rahtu A and Gordon R G 2003 *Nat. Mater.* **2** 749
[23] Hrapovic S, Liu Y, Enright G, Bensebaa F and Luong J H T 2003 *Langmuir* **19** 3958